Mutual Voronoi Tessellation in Spoke Pattern Convection

Stefano Mazzoni,* Fabio Giavazzi,† Roberto Cerbino,† Marzio Giglio, and Alberto Vailati‡

CNR-INFM and Dipartimento di Fisica, Università degli Studi di Milano, via Celoria 16, 20133 Milano, Italy

(Received 11 October 2007; published 6 May 2008)

Planar cellular networks are made of polygonal cells usually having an average of six sides and trivalent vertices. We analyze the topological properties of spoke patterns observed in the convection of highly viscous fluids. The competition between ascending and descending columns of fluid generates dual networks where on average cells are four sided and vertices tetravalent. This observation identifies a new class of dual networks satisfying a mutual Voronoi relation. The metric of the pattern is dominated by the distance between nearest neighbors vertices of opposite species.

DOI: 10.1103/PhysRevLett.100.188104 PACS numbers: 87.18.Hf, 47.55.P−

Cellular patterns form two-dimensional (2D) space dividing networks where the plane is divided into adjacent and nonoverlapping polygonal cells by a set of lines forming a reticulum [1]. Among space dividing networks, Voronoi diagrams are widely used to describe structures such as basins of predation in ecosystems, the texture of giraffe hide, grain boundaries in materials, and urban districts, just to mention a few examples. The applications of Voronoi diagrams span a variety of fields as different as archaeology, physics, crystallography, linguistics, geology, ecology, marketing, and finance [2,3]. Many topological properties of natural space dividing networks are strongly universal and system-independent. The most ubiquitous topological feature is perhaps trivalency [4]. That is, for the vast majority of space dividing networks, three cell edges join at a vertex, and this further implies that the cells are on average hexagonal.

In this work we investigate the topological properties of the spoke patterns generated by convection in fluids. The patterns are made up of the staggered superposition of two cellular networks like the black and white [B (W)] ones shown in Fig. 1. We show that, at variance with the usual trivalent networks, each network is made up by polygonal cells having an average of four sides and tetravalent vertices. The B (W) networks are dual; that is, each vertex of a network is surrounded by a cell of the other network and vice versa. We identify a model for the mutual configuration of the two networks starting from the following simple observation: points contained inside a cell are closer to the dual vertex at its center than to any other dual vertex. According to the definition of Voronoi domain [2], the cell can be identified with the Voronoi domain associated with the dual vertex. Therefore, each network is the Voronoi diagram generated by vertices of the dual network and the two networks are in a mutual Voronoi relation (MVR). The MVR identifies a new class of Voronoi diagrams with potential applications to the modeling of cellular patterns generated by two mutually interacting populations. In particular, the newly found MVR structures could be useful to achieve a better understanding of convection in the Earth's mantle. This is due to the fact that spoke patterns generated in laboratory experiments on convection in viscous fluids have been recognized to represent a model system mimicking at much smaller length scales some of the features of convective structure inside the Earth's mantle [5]. This has been confirmed by recent numerical simulations on mantle convection which have predicted the presence of spoke pattern structures in the lower mantle of the Earth [6]. We point out that in general our laboratory experiments exhibit many simplifications when compared to convection in a real planet. Numerical simulations of planetary convection predict that the spherical geometry of the mantle, the strong dependence of its viscosity from the temperature, and the presence of tectonic plates or of a rigid lid are all factors affecting the actual structure of the convective planform [7–10], which in general deviates from that of a spoke pattern. These factors are not present in our model system.

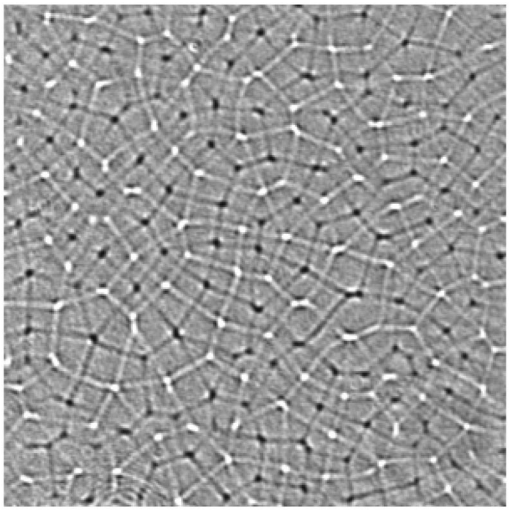

FIG. 1. Shadowgraph image of spoke pattern convection at a solutal Rayleigh number $\mathrm{Ra}_s = 7 \times 10^6$. The image corresponds to a square area of size 10.6 mm × 10.6 mm in real space. The sample thickness corresponds to 0.98 mm.

Spoke patterns are observed in high Rayleigh number convection (either thermal or solutal) of high Prandtl number fluids [5,11–15] and in the bioconvection of populations of bacteria [16–18]. Rayleigh-Bénard convection, besides being affected by the geometry of the sample, is completely determined by two dimensionless numbers: the Rayleigh number $\mathrm{Ra} = \alpha g \Delta T d^3/(\chi\nu)$ and the Prandtl number $\mathrm{Pr} = \nu/\chi$ [19], where g is the gravitational acceleration, ΔT the temperature difference, χ the thermal diffusivity, α the thermal expansion coefficient, ν the kinematic viscosity, and d the sample thickness. Convection can also be induced by creating a gravitationally unstable concentration profile inside a binary mixture. This can be attained by taking advantage of the Soret effect [20]: a thermal gradient induces a mass flow inside a binary mixture, which in turn promotes the formation of a concentration profile. It can be shown [21,22] that there exists a complete analogy between Rayleigh-Bénard convection and Soret driven convection, where Ra and Pr are replaced by the solutal Rayleigh number $\mathrm{Ra}_s = \beta g \Delta c d^3/(D\nu)$ and the Schmidt number $\mathrm{Sc} = D/\nu$. Here β is the solutal expansion coefficient, D the mass diffusion coefficient, and Δc the Soret induced concentration difference across the sample thickness.

In this work we take advantage of the peculiar properties of a suspension of silica nanoparticles in water, commercially known under the brand name LUDOX®. The nanoparticles have a radius of about 11 nm and their weight fraction concentration is 4.1%. At this concentration, the suspension has a negative Soret coefficient $S_T = -3.41\ \mathrm{K}^{-1}$, measured at 25 °C. The mass diffusion coefficient $D = 2.2 \times 10^{-7}\ \mathrm{cm}^2/\mathrm{s}$ is much smaller than the thermal diffusivity $\chi = 1.48 \times 10^{-3}\ \mathrm{cm}^2/\mathrm{s}$. This implies that the high Ra_s needed to induce spoke pattern convection can be attained by imposing a modest temperature gradient to the suspension by heating from above. Moreover, the use of a suspension of nanoparticles allows one to attain a high Schmidt number $\mathrm{Sc} = 3.7 \times 10^4$. A horizontal layer of the suspension is contained within a Rayleigh-Bènard thermal gradient cell [23]. The sample thickness can be changed from 1 mm up to 2.9 mm. The applied temperature difference can be changed from a fraction of a K up to about 20 K. The corresponding range of Ra_s is 10^6–10^9. The convective flow is visualized by means of a shadowgraph technique [24], where a collimated, vertical (parallel to the thermal gradient) light beam impinges on the sample through transparent sapphire windows. The intensity of the shadowgraph image is proportional to the local perturbations of index of refraction of the sample, in turn determined almost entirely by the concentration of the colloidal particles, transported by convection flow. Figure 1 shows a shadowgraph image of a spoke pattern obtained at $\mathrm{Ra}_s = 7 \times 10^6$. The B (W) vertices correspond to upwelling (downwelling) columnar flow of poorly (highly) colloid concentrated sample. The B (W) edges correspond to ridges located near the bottom (top) plate that convey fluid into the columnar flows. Therefore the structure of the pattern is three dimensional, and images like Fig. 1 show a 2D projection of the pattern onto a horizontal plane. Quite remarkably, the observed convective flow takes the form of two dual space dividing networks, where the mean number of sides per cell $\langle s\rangle$ and the mean number of edges joining into vertex $\langle z\rangle$ are close to 4. This is apparent from Fig. 2, which shows the cell shape frequency distribution and the vertex coordination frequency distribution of the networks shown in Fig. 1. B (W) columns in the histograms refer to the B (W) networks of Fig. 1. Histograms are both peaked at four edges.

A first understanding of the topological properties of the spoke pattern can be attained by means of Euler's formula (1). Euler's formula relates the average number of sides per cell $\langle s\rangle$ and the average number of edges joining into a vertex $\langle z\rangle$. For a planar space dividing networks characterized by a large number of cells it states that

$$\frac{1}{\langle s\rangle} + \frac{1}{\langle z\rangle} = \frac{1}{2}. \tag{1}$$

In a usual space dividing network with $z = 3$ the formula implies that $\langle s\rangle = 6$. A dual space dividing network can be constructed from the primal one by taking one point inside each cell and by joining points located within neighboring cells. By construction $\langle s'\rangle = \langle z\rangle$ and $\langle z'\rangle = \langle s\rangle$, where the prime denotes the dual network [2]. This implies that for a trivalent network the dual network is made entirely by triangular cells with $\langle z\rangle = 6$. In the case of a spoke pattern Euler's formula applies independently to the B (W) polygonal networks. Since each B vertex is contained inside a W cell, and vice versa, the B and W networks are dual. From Fig. 1 it is apparent that occasionally more than one B vertex is contained inside a W cell, and vice versa. However, these slight deviations from

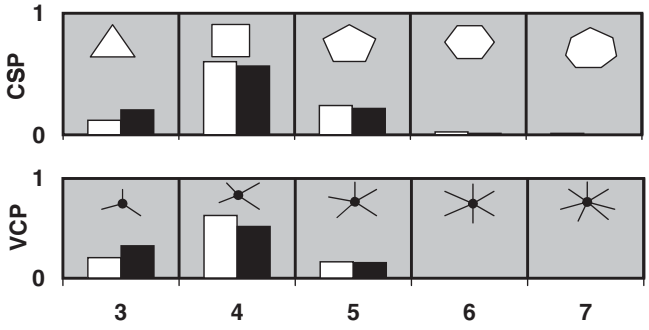

FIG. 2. Cell shape probability (CSP) distribution and vertex coordination probability (VCP) distribution of the B (W) cellular patterns shown in Fig. 1. The B (W) bars correspond to B (W) polygons and vertices in Fig. 1. The total numbers of cells are $C_B = 83$ and $C_W = 83$. The total numbers of vertices are $V_B = 83$ and $V_W = 73$. Cells and vertices were identified by visual inspection of the image. Incomplete cells near the boundary of the image were not considered in the analysis.

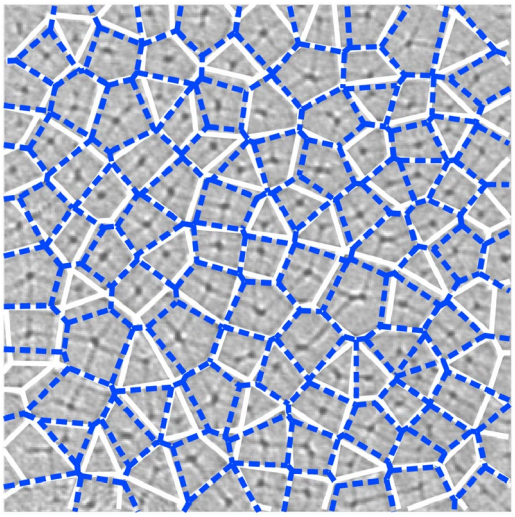

FIG. 3 (color online). Shadowgraph image of the spoke pattern shown in Fig. 1 superimposed to two reconstructions of the white mesh of the diagram. The solid line white network represents a reconstruction of the white mesh obtained by joining the white vertices of Fig. 1. The dashed-line network represents the Voronoi reconstruction of the white mesh using the black vertices of Fig. 1 as generator points.

duality do not alter significantly the topological properties of the patterns. Duality implies that $\langle s_W \rangle = \langle z_B \rangle$ and $\langle s_B \rangle = \langle z_W \rangle$. Moreover, the two networks in a spoke pattern are statistically equivalent; that is, their topological variables are distributed in the same way. Therefore $\langle s_W \rangle = \langle s_B \rangle$ and $\langle z_W \rangle = \langle z_B \rangle$. Duality and statistical equivalence when joined with Euler's formula imply that $\langle s_W \rangle = \langle s_B \rangle = \langle z_W \rangle = \langle z_B \rangle = 4$. This result is in good agreement with the experimental values obtained from the distributions in Fig. 2, where the average values correspond to $\langle s_B \rangle = 4.20$, $\langle s_W \rangle = 4.04$, $\langle z_B \rangle = 3.83$, and $\langle z_W \rangle = 3.95$. Euler's formula is obeyed exactly by the two networks in Fig. 1 as $1/\langle s_B \rangle + 1/\langle z_B \rangle = 0.50$ and $1/\langle s_W \rangle + 1/\langle z_W \rangle = 0.50$.

The most striking topological feature of the spoke pattern is that, given the positions of the vertices of the network of one species, one is able to reconstruct the full structure of the other network. This can be achieved by using the well-known Voronoi tessellation algorithm [2]. In 2D Voronoi tessellations, the plane is divided into polygonal cells which are generated by a set of points. The cells are composed by points that are closer to the corresponding generator than to any other generator. The network shown with a solid white line in Fig. 3 shows a reconstruction of the W network obtained by joining the white vertices of a spoke pattern with segments. The dashed-line network of Fig. 3 shows a reconstruction of the same W network obtained by using the B vertices, whose position is assigned by visual inspection, as generator points of a Voronoi diagram. Although some discrepancies are apparent in Fig. 3, the Voronoi reconstruction mirrors quite closely the original W network. A similar reconstruction of the B network can be obtained from the Voronoi diagram generated by the W vertices. Quite interestingly, spoke pattern convection represents one of the few experimental systems where both the Voronoi diagram and its generator points can be visualized directly at the same time. Figure 3 provides clear evidence that each network in a spoke pattern is generated by the Voronoi tessellation originated by the vertices of the dual network. We will refer to this property as mutual Voronoi relation. The MVR identifies a new class of degenerate Voronoi diagrams where the dual diagram has the same topological properties of the primal

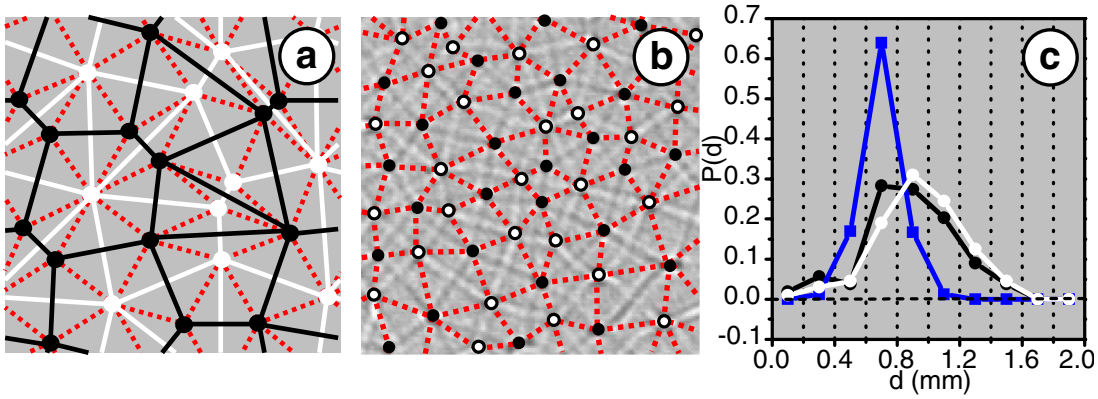

FIG. 4 (color online). (a) Computer-generated MVR diagram showing the symmetries in the position of neighboring vertices of the B (W) networks. The dotted line represents the rhomb tiling obtained by joining nearest neighbors vertices of opposite species. (b) Central portion of Fig. 1 superimposed to a reconstruction of the rhomb tiling (dotted line). The reconstruction has been obtained by joining nearest neighbors vertices of different species. The tiles have a quadrilateral shape with perpendicular diagonals. (c) Frequency distributions for the distance d between neighboring vertices. The square points correspond to the distribution for the distance between vertices of unlike species BW, while the black and white circle points correspond to like species. Data points represent the probability of finding a distance between vertices in the range marked by the vertical dotted lines. The range spans 0.2 mm and represents the intrinsic resolution determined by the size of the vertices in Fig. 1.

one. Figure 4(a) shows two networks in mutual Voronoi relation generated for the purpose of illustration. The MVR implies that each B edge acts as a symmetry axis for a W edge and vice versa. The set of four vertices at the end of the two edges forms a rhomb. Therefore, an equivalent tessellation of the plane involving just a single space dividing network can be constructed by tiling the plane with rhombs. The rhomboidal tessellation is shown by the dotted line in Fig. 4(a). Since every couple of adjoining rhombs share a side, the side of the rhombs has to be equal for all the tiles in the diagram. Therefore, the diagram is dominated by one characteristic length scale, represented by the distance between nearest neighbors vertices of different species.

In order to assess how well the experimental data are described by the ideal rhomboidal tessellation we have attempted a reconstruction of the rhombic network from the central portion of Fig. 1 by joining neighboring vertices of different species. The reconstructed network, shown in Fig. 4(b), is entirely made by quadrilateral cells. All the cells are convex, with the exception of two chevron-shaped ones. The diagonals of all cells, represented by one black edge and one white edge of the spoke pattern, are perpendicular. To verify whether the quadrilateral tessellation exhibits a dominant length scale we have calculated the frequency distributions for the length of sides and diagonals of the quadrilaterals. The distributions have been evaluated by measuring the distances d_{BW} between neighboring vertices of different species and the distances d_{BB} and d_{WW} between neighboring vertices of like species for the pattern shown in Fig. 1. The distribution for d_{BW} is represented by the square points in Fig. 4(c). The black (white) circle points in Fig. 4(c) show for comparison the frequency distributions for d_{BB} and d_{WW}. Figure 4(c) clearly shows the presence of sharp peak of width $\sigma_{BW} = 0.13$ mm for d_{BW} and of two less pronounced peaks of width $\sigma_{BB} = 0.27$ mm and $\sigma_{WW} = 0.26$ mm for d_{BB} and d_{WW}, respectively. Therefore, the frequency distribution for the side of the quadrilaterals is about a factor of 2 narrower than that for their diagonals and d_{BW} represents a dominant length scale for the spoke pattern.

In summary, we studied the spoke pattern exhibited by a highly viscous convecting fluid at high Rayleigh numbers. We identified a novel class of patterns made up by two staggered networks, where each network can be obtained from the other one by means of a Voronoi construction. This unusual mutual Voronoi relation is shown to be dramatically different from the most known case of generic Voronoi diagrams: on the average, the network cells are quadrilateral, the vertices tetravalent, and some short-range order must be present.

We believe that the predictive nature of our findings might contribute to achieve a better understanding of convection in the lower mantle of the Earth, where the spoke pattern has been observed as a result of complex 3D numerical simulations [6].

We thank P. Cicuta and P. J. Lu for discussion.

*Current address: European Space Agency–ESTEC Keplerlaan 1, 2200AG Noordwijk AZ, The Netherlands.
†Current address: Dipartimento di Chimica, Biochimica e Biotecnologie per la Medicina, Università degli Studi di Milano, via F. Cervi 93, 20090 Segrate (Milano), Italy.
‡Corresponding author.
alberto.vailati@unimi.it

[1] G. Schliecker, Adv. Phys. **51**, 1319 (2002).
[2] A. Okabe, B. Boots, K. Sugihara, and S. N. Chiu, *Spatial Tessellations: Concepts and Applications of Voronoi Diagrams* (Wiley, Chicester, 2000).
[3] B. De Lacy Costello *et al.*, Int. J. Bifurcation Chaos Appl. Sci. Eng. **14**, 2187 (2004).
[4] J. Stavans, Rep. Prog. Phys. **56**, 733 (1993).
[5] D. P. McKenzie and F. Richter, Sci. Am. **235**, 72 (1976).
[6] F. Dubuffet and D. A. Yuen, Geophys. Res. Lett. **27**, 17 (2000).
[7] J. T. Ratcliff, P. J. Tackley, G. Schubert, and A. Zebib, Phys. Earth Planet. Inter. **102**, 201 (1997).
[8] H. P. Bunge, M. A. Richards, C. Lithgow-Bertelloni, J. R. Baumgardner, S. P. Grand, and B. A. Romanowicz, Science **280**, 91 (1998).
[9] C. C. Reese, V. S. Solomatov, J. R. Baumgardner, and W. -S. Yang, Phys. Earth Planet. Inter. **116**, 1 (1999).
[10] M. Monnereau and S. Quere, Earth Planet. Sci. Lett. **184**, 575 (2001).
[11] F. H. Busse and J. A. Whitehead, J. Fluid Mech. **66**, 67 (1974).
[12] J. A. Whitehead and B. Parsons, Geophys. Astrophys. Fluid Dyn. **9**, 201 (1978).
[13] F. H. Busse, Acta Mech. **4**, 11 (1994).
[14] A. La Porta and C. M. Surko, Phys. Rev. Lett. **80**, 3759 (1998).
[15] R. Cerbino, A. Vailati, and M. Giglio, Phys. Rev. E **66**, 055301(R) (2002).
[16] J. R. Platt, Science **133**, 1766 (1961).
[17] I. M. Jánosi, J. O. Kessler, and V. K. Horváth, Phys. Rev. E **58**, 4793 (1998).
[18] A. Czirók, I. M. Jánosi, and J. O. Kessler, J. Exp. Biol. **203**, 3345 (2000).
[19] T. E. Faber, *Fluid Dynamics for Physicists* (Cambridge University, Cambridge, England, 1995).
[20] S. R. De Groot and P. Mazur, *Nonequilibrium Thermodymanics* (North-Holland, Amsterdam, 1962).
[21] V. Degiorgio, Phys. Rev. Lett. **41**, 1293 (1978).
[22] A. Ryskin, H. W. Müller, and H. Pleiner, Phys. Rev. E **67**, 046302 (2003).
[23] S. Mazzoni, R. Cerbino, D. Brogioli, A. Vailati, and M. Giglio, Eur. Phys. J. E **15**, 305 (2004).
[24] G. S. Settles, *Schlieren and Shadowgraph Techniques: Visualizing Phenomena in Transparent Media* (Springer, Berlin, 2001).